Decahedral-shaped anatase titania photocatalyst particles: synthesis in a newly developed coaxial-flow gas-phase reactor

Marcin Janczarek[a,b,*], Ewa Kowalska[a], Bunsho Ohtani[a]

[a] Institute for Catalysis, Hokkaido University, Sapporo 001-0021, Japan

[b] Department of Chemical Technology, Gdansk University of Technology, Gdansk 80-233, Poland

*Corresponding author. E-mail address: mjancz@pg.gda.pl (M. Janczarek)

Abstract

Decahedral-shaped anatase particles (DAPs) were prepared by a gas-phase process consisting of titanium(IV) chloride oxidation. The use of a coaxial-flow gas-phase reactor resulted in high reaction yield (ca. 70%) and good reproducibility of DAPs production. The influence of controlled and resultant preparation parameters on the process course and on DAPs properties (such as specific surface area, particle size and particle morphology) is discussed in detail. Correlations between preparation parameters and product properties indicated the best conditions for obtaining DAPs of high quality and thus with a high level of photocatalytic activity for various reaction systems.

Keywords: anatase titania, decahedral-shaped particles, gas-phase synthesis, coaxial-flow reactor, photocatalytic activity

Nomenclature

$C_{TiCl4(g)}$	concentration of $TiCl_4$ vapor in gas phase (vol%)	*SPS*	secondary particle size (nm)
F	amount of powder collected from the glass-fiber filter (g)	*SSA*	specific surface area (m^2 g^{-1})
L	length of the reaction zone (m)	*T*	amount of powder collected from the reaction tube (g)
LSR	line speed ratio of reactant gases	T_F	furnace temperature (K)
p	internal pressure (kPa)	t_{res}	residence time (s)
PAR	particle aspect ratio	*U*	average volumetric flow rate of the gas mixture (m^3 s^{-1})
PPS	primary particle size (nm)	U_{Ar}	volumetric flow rate of argon (m^3 s^{-1})
PSD	particle shape distribution (%)	U_{O2}	volumetric flow rate of oxygen (m^3 s^{-1})
PSH	particle size heterogeneity	$U_{TiCl4(g)}$	volumetric flow rate of $TiCl_4$ vapor (m^3 s^{-1})
r	radial distance (m)	$U_{TiCl4(l)}$	volumetric flow rate of $TiCl_4$ liquid (m^3 s^{-1})
R	reaction tube radius (m)	η	viscosity of the gas mixture (Pa s)
Re	Reynolds number	ρ	density of the gas mixture (kg m^{-3})

1. Introduction

Titanium(IV) oxide (TiO_2; titania) is a well-known photocatalyst with widespread applications including treatment of pollutants and solar energy conversion [1-2]. Improvement in its photocatalytic activity is important for increasing its use in photocatalysis in technological fields. Two main limitations affect the photocatalytic application of titania. Firstly, only ultraviolet light is able to induce a photocatalytic reaction on titania. Secondly, the recombination of photoexcited charge carriers (electron (e^-)–holes (h^+)), which reduces quantum efficiency, has not been controlled [3]. Many studies have been performed to obtain visible light activity by modification of titania with metal and non-metal elements [4-7]. The second limitation can be overcome by surface modification of titania with noble metals and their compounds that inhibit the charge recombination by increasing the transfer of photoexcited electrons from titania to substrates [5,8-10]. Another approach is the preparation of p-n junction photocatalysts (e.g., nickel oxide/titania) to induce an internal electric field in the contact between p-type and n-type materials, which can increase e^-–h^+ separation [11]. A promising strategy to overcome this limitation is the preparation of single-crystalline anatase titania particles with a small amount of crystalline defects, which are thought to be recombination centers (deep electron traps), and thus with a high level of

photocatalytic activity. In addition, the difference in surface energies of the conduction and valence bands of different crystal facets of titania can promote the separation of electrons and holes [12]. The shape of an anatase titania single crystal, which determines the type of the exposed crystal facet, has recently been recognized as a potential key factor influencing photocatalytic efficiency and selectivity [13-16].

Decahedral-shaped anatase titania particles (DAPs) have recently been classified as a photocatalytic material with a high level of photocatalytic activity [17-19]. The presence of two additional (in comparison to natural anatase titania crystals of octahedral shape) square {001} facets in DAPs and their relation to {101} facets are expected to play a crucial role in the enhancement of photocatalytic efficiency for different reaction systems [20]. According to the Wulff construction theory, surface energy minimization is the main factor determining the shape of faceted crystals. The total surface energy decreases until the minimum point in given growth conditions [21]. The development of a reaction environment that would allow pure DAPs with tunable properties dedicated to proper reaction systems to be obtained is important for further applications and scaling up of the process. Two main types of methods for preparation of DAPs have been reported. The first approach is known as a wet-chemistry route related to hydrothermal reactions. This approach involves the application of fluorine-containing species (e.g., hydrogen fluoride, ammonium fluoride, titanium(IV) fluoride and tetrafluoroborate ion) as morphology-controlling agents to prevent the formation of more thermodynamically stable octahedral anatase titania particles (OAPs) exposing only {101} facets [22-33]. Other compounds including polyvinyl alcohol [34,35] and carbonate ions generated during decomposition of urea have also been used to control the shape [20]. However, the disadvantage of this approach is strong adsorption of shape-control reagents (e.g., fluoride ions) on the crystal surface or their doping into the lattice, which may result in a decrease in photocatalytic activity [34]. Furthermore, at high temperatures, fluorine

compounds generate toxic and corrosive products, making scaling-up of the preparation process difficult. The second approach, which is based on a gas-phase reaction, is devoid of those limitations. The first gas-phase crystallization of titania nanoparticles with a decahedral shape was performed in an aerosol reactor from titanium alkoxide [36,37]. However, the photocatalytic activity of this material was not evaluated. Another method for producing DAPs in a gas phase was developed by our group [17-19]. The main idea of this method is to apply rapid heating and quenching, which may preclude formation of octahedral anatase particles, of a gas reaction mixture. Generally, vapor of titanium(IV) chloride ($TiCl_4$) was liberated by bubbling of argon (200 mL min^{-1}) into a $TiCl_4$ solution at 358 K, and then vapor was mixed with oxygen (1200 mL min^{-1}) and fed into a quartz glass tube heated from the outside. Two variants of this experimental system depending on the source of heat have been used. In one system, a quartz glass tube was rotated around the cylindrical axis for homogeneous temperature distribution and was heated by an oxyhydrogen flame burner at 1573 K [17,18]. In the other system, an infrared furnace equipped with platinum foil located in the center part of quartz glass tube was used to assure a more stable and precise temperature in the heating zone [19]. DAPs obtained by using these two systems showed photocatalytic activities for various reaction systems that were comparable to or higher than those of commercially available samples with high photocatalytic activities such as P25 (Evonik) and FP-6 (Showa Denko Ceramics).

DAPs have a high potential as a commercial material for efficient photocatalysis. The purpose of the present study was to determine correlations between preparation parameters and titania properties and thus to find the best conditions for obtaining DAPs with a high level of photocatalytic activity, high yield of powder production and a high degree of homogeneity of particles. The experiments were performed in a newly developed coaxial-flow gas-phase reactor that enables a continuous and stable flow of $TiCl_4$ vapor to be maintained. In the

previous reaction systems [17-19], the vapor of $TiCl_4$ was liberated by bubbling argon into $TiCl_4$ solution what does not allow precise control of $TiCl_4$ vapor concentration. In the proposed experimental set up, a portion of liquid $TiCl_4$ was continuously fed to a vaporizer with a controlled flow rate and argon was passed through the vaporizer as the carrier gas for $TiCl_4$ vapor. $TiCl_4$/Ar mixture was fed at the centre of the tube as close as possible to the reaction zone filled with oxygen. Proposed solution delays contact of $TiCl_4$/Ar and oxygen streams to ensure rapid reaching of target temperature of reaction mixture. The reaction was carried out with an excess of oxygen. The premixing of $TiCl_4$ vapors and dried O_2 as it is realized [38,39] to avoid low temperature hydrolysis is not necessary because no water vapor exists in the reaction environment. The control of $TiCl_4$ vapor concentration and residence times of gaseous reagents in the reaction zone is crucial for precise tuning of the properties of DAPs. Another advantage of the continuous feeding is easy adaptation of this method to industrial conditions facilitating scaling up of the preparation process.

2. Experimental

2.1 Synthesis of DAP-containing samples

DAP-containing powders were prepared in the experimental system shown in Figure 1. A 7.5-mL portion of liquid $TiCl_4$ was continuously supplied to a vaporizer vessel (1) by an automatic syringe feeder (2) with a specified flow rate (0.6–6.0 mL h^{-1}). Simultaneously, argon (Ar; 75 mL min^{-1}) was passed through the vaporizer as the carrier gas for $TiCl_4$ vapor. It was necessary to keep the constant temperature for argon and $TiCl_4$ liquid (453 K) (T-1) higher than boiling point of $TiCl_4$ (410 K). In such conditions, a mixture of two gases passed through the preheating zone (473 K) (T-2) to a quartz reaction tube (4). Oxygen (O_2; 500–2000 mL min^{-1}) was delivered to a preheating zone tube (3) without contact with the Ar/$TiCl_4$ stream, which was provided by a small tube placed coaxially inside the preheating zone tube directly to the reaction zone of the quartz reactor (T-3). The reaction mixture was heated

(1173–1473 K) (T-3) by an infrared furnace (5) (ULVAC-Riko) equipped with a temperature controller. The central part of the quartz reactor tube (45 cm in length, 3.8 cm in diameter) was wrapped with platinum foil (3 cm in width) (6) and heated by infrared lamps. A thermocouple was connected to the platinum foil, and the intensity of the infrared light was regulated precisely by the temperature controller. The temperature reached the required temperature for heating in the reaction tube area in contact with the platinum foil (T-3). In other parts of the reaction tube, the temperatures were much lower to assure rapid heating and quenching of the gas reaction mixture. To provide, at the same time, stable conditions for crystallization and high yield of powder, a low vacuum (p=95 kPa) was applied by connecting a vacuum pump (7) (KNF-LAB, type Laboport N810FT.18) to an outlet of a filter tube. The vacuum was adjusted and controlled by a pressure regulator (8) installed near the inlet of the vacuum pump. The pressure regulator was connected to a desiccator (9) with silica gel packing to prevent the introduction of moisture from air. A scrubber system was used to remove liberated chlorine and remains of $TiCl_4$ from the exhaust gas. A shower-type scrubber (10) was packed with glass Raschig rings. An aqueous solution of sodium hydroxide (2 mol L^{-1}) in a reservoir (13) was circulated by a peristaltic pump (11) equipped with two rotary modules. Titania powder was collected from inside the reaction tube and from a glass-fiber filter (12) (Whatman) set tightly in a filter tube to prevent leakage of the powder to the vacuum pump. Prepared titania samples were washed thoroughly with water to remove residual chlorine and separated from the aqueous phase by centrifugation (10000 rpm, 25 min). The washing procedure was repeated five times. Subsequently, water was removed by freeze-drying under vacuum for 24 h.

2.2 Characterization

Gas-adsorption measurements of prepared titania samples were performed on a Yuasa Ionics Autosorb 6AG surface area and pore size analyzer. Specific surface area (SSA) was

estimated from nitrogen adsorption at 77 K using the Brunauer–Emmett–Teller equation. Primary particle size (*PPS,* crystallite size), phase content and particle aspect ratio were determined through X-ray diffraction measurements using Cu-Kα radiation on a Rigaku SmartLab. *PPS* was estimated by the Scherrer equation using corrected full width at half maximum (FWHM) of the most intense XRD peaks of anatase at ca. 25.3 deg. The value of 0.891 was used as a constant in the Scherrer equation. Particle aspect ratio (PAR, d_{001}/d_{101}) was calculated by the quotient of crystallite sizes related to anatase XRD peaks (004) and (101) corresponding to d_{001} and d_{101} values, respectively. Non-crystalline content, i.e., amorphous titania and water, was calculated by the internal standard method, in which highly crystalline nickel oxide (NiO) was used as the standard, by mixing titania (80wt%) and NiO (20wt%) samples. The morphology of the obtained DAP-containing samples was evaluated by field emission scanning electron microscopy (FE-SEM; JEOL JSM-7400F). Particle shape distribution (*PSD*) and secondary particle size (*SPS*) were estimated from FE-SEM images by visual analysis. The following classification was used for visual recognition of titania particles. DAPs were defined as particles having a decahedral shape without visible defects (Figure 2A). The probability of the occurrence of a pure decahedral structure is 50% since only one side is observed. Semi-DAPs were defined as particles with a decahedral shape and noticeable defects (e.g., mounds (Figure 2B)) located on the facets. Semi-DAPs also include aggregates (Figure 2C) and broken decahedral particles (Figure 2D), which were counted as single particles. Others were defined as particles with a shape different from decahedral (regular or irregular), as shown in Figure 2E.

2.3 Photocatalytic reactions

The photocatalytic activity of products was evaluated in two reaction systems: (a) oxidative decomposition of acetic acid (CO_2 system) and (b) dehydrogenation of methanol with in-situ platinum photodeposition under deaerated conditions (H_2 system)

[17]. The commercial photocatalyst Degussa (Evonik) P25 was used as a reference sample because of its high level of activity in various photocatalytic reactions ensuring clear discussion of the influence of reaction parameters on photocatalytic activity of DAPs [40]. Sample powder (50 mg) was placed in a test tube of ca. 35 mL in volume and suspended in water (5.0 mL) containing 5.0vol% acetic acid (a) or 50vol% methanol (b). In the case of system (b), hydrogen hexachloroplatinate(IV) ($H_2PtCl_6 \cdot 6H_2O$) was added for 2.0wt% platinum loading, and the suspension was purged with Ar before irradiation to remove oxygen from the system. For both systems, the test tubes were sealed with rubber septa and irradiated with UV/visible light (λ>290 nm) using a 400-W high-pressure mercury lamp (Eiko-sha) under the condition of magnetic stirring at 1000 rpm. The reaction temperature was kept at 298 K using a thermostated water bath. To analyze the progress of reactions, amounts of CO_2 (a) and H_2 (b) were measured using a TCD gas chromatograph (Shimadzu GC-8A) equipped with two GC columns: Molecular Sieve 5A and Porapak-Q for H_2 and CO_2 analyses, respectively. Gas samples were taken to the analysis every 20 min. Total time of photocatalytic activity test was 60 min.

3. Results and discussion

3.1 Preparation parameters and flow character

Seven preparation parameters were adjusted to control the properties of the final product, i.e., flow rate of liquid $TiCl_4$, flow rate of O_2, flow rate of Ar, furnace temperature (T_F), internal pressure, temperature of the vaporizer and temperature of the preheating zone. Using these controlled parameters, two main resultant parameters were defined: concentration of $TiCl_4$ vapor in gas phase ($C_{TiCl4(g)}$) and line speed ratio (*LSR*). $C_{TiCl4(g)}$ was related to the gas mixture in the reaction zone corresponding directly to the molar ratio of $TiCl_4/O_2$. *LSR* of reactant gases was obtained from the following equation (1):

$$LSR = \frac{U_{TiCl_4} + U_{Ar}}{U_{O_2}}, \qquad (1)$$

where $U_{TiCl4(g)}$, U_{Ar}, and U_{O2} are line speeds of $TiCl_4$ vapor, Ar and O_2 respectively. Changes in $C_{TiCl4(g)}$, *LSR* and furnace temperature (T_F) directly influenced the properties of obtained titania powders. To determine the flow character of the gaseous mixture, Reynolds number (*Re*) was calculated by the following equation:

$$Re = \frac{U\ R\ \rho}{\eta}, \qquad (2)$$

where *Re* is Reynolds number, *U* is average line speed of the gas reaction mixture ($U = U_0/2$, where $U_0 = U_{TiCl4} + U_{Ar} + U_{O2}$), *R* is reaction tube radius (0.019 m), ρ is density of the gas mixture and η is viscosity of the gas mixture.

Table 1 shows that the gas flow had a laminar character (*Re*:(5.3–21.5); *Re*<2100) for all conditions. Taking into consideration a laminar tubular flow, the line speed of the gas reaction mixture and consequently residence time (t_{res}) are described by a parabolic distribution (supplementary data, Figure S1) [41]:

$$U(r) = 2\,U\,(1 - (r/R)^2), \qquad (3)$$

where *U(r)* is line speed of the gas reaction mixture in a radial distance *r* (calculations were related to the centerline position, $r = 0$) and *U* is average line speed of the gas reaction mixture. Corresponding t_{res} values were calculated from equation (4):

$$t_{res} = \frac{L}{U}, \qquad (4)$$

where *L* is length of the reaction zone (0.03 m).

Among the resultant parameters, it was found that gas flow (*Re* and t_{res}) was influenced the most by *LSR*. Although the flow was laminar, the wide range of *Re* values, i.e., 5.3–21.5, indicated different degrees of flow homogeneity. In general, residence times of gaseous

reactants are directly related to *Re* values. Thus, the change in *LSR* from 0.04 to 0.16 also resulted in a change in t_{res} from 0.46 to 1.83 s. The influence of other parameters ($C_{TiCl4(g)}$ and T_F) on the character of the flow was not significant. Similar results were reported by Ahonen et al. [37] in preparations of titania in a gas-phase system (aerosol reactor) from $TiCl_4$, i.e., the obtained *Re* of ca. 25 confirmed a laminar character of the flow, and the change in furnace temperature (1273–1473 K) did not greatly influence resultant parameters. It should be pointed that the residence time in the reaction zone varied with every change in flow rate of introduced gases. To ensure the constant t_{res} it would be favorably to use inert gases for compensating the changes in oxygen and $TiCl_4$/Ar flow rate. Detailed discussion on the correlation between preparation conditions and properties of DAPs requires analysis of the influence of flow homogeneity and residence time as the important factors describing reaction conditions in the gas phase.

3.2 Reaction yield and product distribution in a reactor

The reaction yield of titania and the ratio of the amounts of powder collected from the glass-fiber filter (*F*) and reaction tube (*T*) are important factors for scaling up. Products of good quality, i.e., high DAP content, are obtained at a high *F*/*T* ratio, since titania powder collected from the reaction tube has high heterogeneity. The conditions in the whole tube are inhomogeneous and depend on the position inside the tube, i.e., different distribution of temperature. Thus, the properties of the powder collected from the reaction tube depend additionally on the total time of heating of the reaction tube. This heterogeneity makes unequivocal description of the preparation conditions for titania collected from the reaction tube impossible. On the other hand, the preparation conditions for titania powder obtained from the glass-fiber filter (in contradistinction to that from the reaction tube) can be precisely described since the conditions inside the filter are the same for each portion of prepared powder. Figure 3 shows the relationships of preparation parameters with reaction yield and

F/T ratio. The maximum reaction yield (67.7%) and the highest *F/T* ratio (2.0) were obtained with the following parameters: $C_{TiCl4(g)}$ = 0.86vol%, *LSR* = 0.08 and T_F = 1373 K. Change in $C_{TiCl4(g)}$ had almost no influence on either of the parameters, while increases in *LSR* and T_F resulted in increases in reaction rate and *F/T* ratio up to maximum values of 67.7% and 2.0, respectively, at *LSR* of 0.10 and T_F of 1373 K. Further increase in *LSR* (≥ 0.98) caused decreases in reaction yield and *F/T* ratio, indicating an optimal line speed ratio of 0.08 in the case of this reactor. An excessively high line speed ratio was thought to be detrimental for reaction efficiency due to an insufficient amount of oxygen being provided for $TiCl_4$ oxidation. Similarly, the decrease in the amount of titania collected in the glass-fiber was probably caused by an excessively long t_{res} of 1.83 s (almost twice longer than that at optimal *LSR*), enhancing titania attachment to the wall of quartz tube.

In contradistinction to the influence of *LSR*, elevation of the furnace temperature resulted in an increase in reaction yield that reached a plateau at 1333 K, indicating that the high-temperature conditions are still favorable for stability of the DAP crystallization process. On the other hand, *F/T* ratio reached a maximum value of ca. 2 at 1373 K, suggesting that excessively high T_F (similar to high *LSR*) could result in particle attachment to the quartz tube wall.

The courses of all dependences shown in Figure 3a-c for both parameters are almost the same, indicating a direct correlation between them, which is shown in Figure 3d. This observation is not surprising since insufficient conditions for the reaction, e.g., low temperature and/or low line speed ratio, result in incomplete reaction and in production of an insufficient amount of product to be transferred to the receiver (glass-fiber filter).

The influence of residence time on these two parameters was also examined, and data are shown in Figure 4. The highest values of reaction yield and *F*/*T* ratio were obtained for an optimal value of t_{res} in the range of 0.8 to 1.0 s. The points with the lowest values of both

factors (marked as (x)) correspond to the sample prepared at the lowest furnace temperature of 1173 K, which was insufficient for complete reaction. In summary, the optimal furnace temperature (ca. 1373 K) and homogeneity of reaction mixture flow with the optimal range of *LSR* (0.08-0.1) and corresponding t_{res} (0.8-1.0 s) determine the reaction yield and quality of products (*F*/*T* ratio). To improve the control of DAPs crystallization process additional cooling system for quenching of the final product is being considered [42].

3.3 Specific surface area and particle size

$C_{TiCl4(g)}$ directly influenced the physical properties of DAPs including specific surface area (*SSA*), primary particle size (*PPS*), secondary particle size (*SPS*) and particle size heterogeneity (*PSH*). *PSH* was calculated on the basis of *SPS* distribution: quotient of standard deviation and average value of particle size. The histogram of *SPS* distribution for an exemplary sample was showed in Figure S2, supplementary data.

An increase in $C_{TiCl4(g)}$ induced the formation of particles with smaller *SSA* and larger *PPS* and *SPS*, as shown in Figure 5. The lowest particle size heterogeneity (*PSH* = 0.24) was obtained with 0.86vol% (Figure 6a). Although changes in *LSR* and T_F had no influence on *SSA*, *PPS* and *SPS*, they significantly influenced *PSH*. It was found that *LSR* values equal to or higher than 0.08 and T_F of ca.1373 K are appropriate (Figures 6b, 6c) for low *PSH* of obtained particles. It is notable that T_F of 1373 K resulted in both the highest *F*/*T* ratio and lowest *PSH* of DAPs, confirming the previous assumption that products collected from the filter should be characterized by lower values of *PSH*.

Two main chemical pathways for oxidation of $TiCl_4$ vapor have already been proposed by Pratsinis et al., [43, 44] i.e., $TiCl_4$ can react with O_2 either i) in the gas phase to form TiO_2 or a precursor (oxychloride) or ii) on the surfaces of formed titania particles. An increase in $C_{TiCl4(g)}$ causes an increase in the rate of particle formation, which ensures a sufficient surface area for dominance of surface oxidation [44]. This fact is responsible for the delay in

nucleation bursts, which results in the formation of larger particles. The unnoticeable influence of T_F on particle size may result in contradictory actions between acceleration of $TiCl_4$ oxidation kinetics and coagulation of titania particles.

Heterogeneity of particle sizes is one of the most important factors for the quality of obtained titania particles. Particles were characterized by high *PSH* when they were prepared at high $C_{TiCl4(g)}$, low *LSR* and T_F lower than 1273 K, possibly caused by the local turbulence of flow and/or insufficient temperature for the reaction. The relation between *PSH* and *Re* is shown in Figure 7. An increase in laminarity of the flow (lower values of *Re*) favored particle size homogeneity with only one exception for the most heterogeneous (0.5) sample prepared at the lowest temperature of 1173 K, since low T_F dominated other preparation conditions and resultant properties, as was also confirmed by the lowest reaction yield of only ca. 5%. It must be pointed that scaling up of the experimental setup could result in increase in Reynolds number and finally in higher *PSH* values. It can also cause an acceleration of titania particles coagulation process [45]. Therefore, further study on development of reactor construction will consider this issue.

3.4 Phase content

An example of XRD diffractograms for a DAP-containing sample mixed with an inert standard (NiO, to determine non-crystalline content) is shown in Figure 8. The samples were well crystallized (>90%) and consisted mainly of anatase crystals (ca. 98%) and rutile crystals. Amorphous phase content (after subtracting water content of 1.0-1.5%) was usually in the range of 5–7%. The amorphous content was lowest (not exceeding 2%) in the samples prepared with the highest T_F and lowest $C_{TiCl4(g)}$. The preparation parameters did not almost influence phase composition.

Although anatase thermal stability was suggested in the literature for small crystallites which do not exceed 14-16 nm [46,47], due to the fact that their stability depends on OH_2^- and

OH^- surface adsorbed groups, DAPs of much larger sizes exhibited high stability. High thermal stability of single crystalline anatase particles has recently been reported for octahedral anatase (OAPs) [48] and nanorice anatase particles [49]. It has been suggested that faceted particles, without crystal–crystal attachment points, leads to the minimization of surface energy and consequently to an increase in the activation energy of anatase to rutile transformation [25]. Other possible reason is specific preparation conditions, i.e., very short exposure time (< 2 s) of the reaction mixture to a high temperature (1173–1473 K) insufficient for phase transition (from anatase to rutile). It was found that titania samples collected from the central part of the reaction tube consisted of a smaller amount of anatase (ca. 80%) since their exposure time was significantly longer than that for titania collected from the glass-fiber filter. Another possible reason is a small amount of oxygen deficiencies in faceted DAPs. It is assumed that the presence of oxygen deficiencies accelerates anatase-to-rutile phase transition [37]. The $TiCl_4/O_2$ ratio adjusted by the changing of $C_{TiCl4(g)}$, was in the range of 0.003 to 0.02, indicating an excess of oxygen, which should prevent the formation of oxygen deficiencies. A slightly higher rutile content (ca. 5%) was observed only for samples prepared with a higher $TiCl_4/O_2$ ratio (ca. 0.02).

3.5 Particle morphology

Particle morphology of prepared DAP-containing samples was described by two main parameters: particle shape distribution (*PSD*) and particle aspect ratio (*PAR*). Figure 9 shows the dependence of *PSD* on the main process parameters. It was found that all of the considered preparation parameters influenced *PSD*, and maxima of DAP content (at the minima of semi-DAP content and others) were observed for $C_{TiCl4(g)}$ = 0.86vol%, *LSR* = 0.08 and T_F = 1373 K, which are exactly the same as those for preparation of samples with the highest reaction yield, *F*/*T* ratio and *PSH* (Figures 4 and 5). This suggests that these conditions are the best for obtaining titania particles with the highest content of DAPs. The

amount of particles with an irregular shape ("others") was small and usually did not exceed 10%, with one exception for the most heterogeneous sample prepared at the lowest temperature of 1173 K (40%). The influence of $C_{TiCl4(g)}$ on particle morphology is also shown by SEM images in Figure 10. The existence of two main subgroups for semi-DAP was noticed, i.e., aggregates and particles with mounds on the {001} facets (Figure 10C, D). Their distribution as a dependence of main preparation parameters is shown in supplementary data, Figure S3. A change in $C_{TiCl4(g)}$ had little influence on the content of particle aggregates (4–9%). The smallest aggregate content was observed for *LSR* of 0.08, indicating the existence of an optimal flow with which aggregation is hindered. However, no clear correlation between T_F and aggregate content could be obtained. Particles with mounds on the {001} facets were formed mainly with larger $C_{TiCl4(g)}$ (>1vol%), lower *LSR* (<0.08), and lower T_F, indicating that shorter reaction time at lower temperatures with concentrated titania facilitated formation of deposits on the surface of {001} facets. The presence of mounds is evidence of the predominance of the $TiCl_4$ vapor surface oxidation pathway in the reaction zone at high $C_{TiCl4(g)}$, low *LSR* and low *F*/*T* ratio [44]. Mounds have two possible functions: i) as surface starting points for the growth of new decahedral crystals and ii) as a possible "embryo" of high-index facets as suggested by Jiang et al. [50]. It was reported that the embryo that arose during the gas-phase preparation process resulted in the formation of crystal facets indexed as {105} and {107}. The latter assumption seems more likely for the samples in this study since generated mounds have rather different directions.

The particle morphology of DAP-containing samples was characterized by particle aspect ratio (*PAR*, d_{001}/d_{101}) as shown in supplementary data, Figure S4. *PAR* shows the geometric relations of decahedral crystals and signifies the ratio between surface areas of {001} and {101} facets, i.e., a lower aspect ratio means larger content of {001} facets. *PAR*, determined by XRD, was not changed significantly (0.87-0.95) by any of the preparation parameters.

Only $C_{TiCl4(g)}$ (Figure S5, supplementary data) might control *PAR* in a narrow range, and the minimum value was obtained at ca. 0.9vol%. No clear dependence was observed for other parameters, and the existence of a maximum at *LSR* = 0.06 and slight increase of *PAR* with increase in T_F were observed (Figure S6, supplementary data). Further investigation of particle aspect ratio dependence is currently underway.

3.6 Photocatalytic activity

Photocatalytic activity tests were performed for DAP-containing samples obtained by different preparation conditions in two reaction systems, i.e., CO_2 and H_2 systems. In the CO_2 system (oxidative decomposition of acetic acid), molecular oxygen works as an acceptor of photogenerated electrons, while the photogenerated holes oxidize acetic acid finally to CO_2. In the H_2 system (dehydrogenation of methanol with in-situ platinum photodeposition under deaerated conditions), at the beginning of irradiation, hexachloroplatinic acid is reduced by photoexcited electrons, resulting in the formation of platinum deposits on the surface of the photocatalyst. The presence of platinum as a co-catalyst is a necessary condition for H_2 evolution. In the H_2 system, methanol plays the role of a hole scavenger [10, 51]. Time courses of CO_2/H_2 gas evolution were linear as shown in Figure S7, supplementary data.

The dependence of photocatalytic activities on main DAPs preparation parameters is shown in Figure 11. In the CO_2 system, the maximum photocatalytic activity was observed at $C_{TiCl4(g)}$ of 0.86-vol% and T_F of 1373 K. The pattern of dependence of the CO_2 system in Figure 11a-c resembles that in Figure 9a-c (DAP content), suggesting that particle shape morphology (represented by the content of DAPs) might be the main factor determining photocatalytic activity in the CO_2 system. Figure 12a shows relationship between DAP content and photocatalytic activity in the CO_2 system. Higher DAP content and lower content of particles with mounds favor higher photocatalytic activity in the oxidation of acetic acid (Figure 12). Higher content of particles with mounds is rather advantageous for

photocatalytic activity in the H_2 system. The influence of particle size heterogeneity on photoactivity was also investigated, due to appreciable inverse trends in Figure 6a-c and Figure 11a-c. It was found that an increase in particle size heterogeneity was detrimental for photocatalytic activity in the CO_2 reaction system (supplementary data, Figure S8a). However, the influence of DAP content on photocatalytic activity was more readable than that of particle size heterogeneity.

In the H_2 system, photocatalytic activity increased with an increase in $C_{TiCl4(g)}$, reaching a plateau for 1vol%. On the other hand, high *LSR* and low T_F caused a decrease in the photocatalytic activity, as in the case of trends observed for the quality of samples, i.e., DAP content (Figure 9b-c), *F*/*T* ratio (Figure 3b-c), and inversely proportional to mound-deposited particle content (supplementary data, Figure S3b-c). It is thought that {001} facets are necessary for highly efficient dehydrogenation of alcohols in the presence of co-catalysts.

Although metal deposits (here Pt) were reported to be preferentially formed on the {101} facet, and thus generation of hydrogen is expected on this facet, the presence of a naked {001} facet with higher surface energy was proposed to be necessary for efficient separation of charge carriers [12]. It is thought that alcohol molecules would be more easily adsorbed on the {001} facet (more reactive one with 100% five-coordinated Ti (Ti_{5c}) atoms) [24] or/and better separation of charge carriers (by simultaneous transfer of electrons and holes to different facets) could facilitate redox reactions, as was reported for DAPs possessing naked {001} and Pt-modified {101} facets [52]. It was reported that DAPs possessing Pt nanoparticles uniformly deposited on both facets showed much lower photocatalytic activity than that of DAPs with Pt nanoparticles selectively deposited on {101} facets [52], similar to less active OAPs possessing only {101} facets [53]. In the present study, platinum particles were deposited on both facets of DAPs (Figure S9, supplementary data) and their photocatalytic activity in H_2 system was significantly higher than OAPs prepared according to

ref. 53. The results of present study, however, suggested that the activity dependence cannot be simply interpreted by the exposure of facets and/or platinum deposit location, considering the influence of the content of particles with mounds.

Other resultant parameters including *SSA* and *PPS* are related mainly to values of $C_{TiCl4(g)}$. No clear correlation exists between *SSA* and photocatalytic activity in the H_2 system (supplementary data, Figure S8b). In the CO_2 system, it is possible to indicate the maximum of photocatalytic activity at *SSA* = 16 $m^2 g^{-1}$. The particle aspect ratio was varied by changing preparation conditions in a very narrow range, and it is therefore difficult to find a correlation between *PAR* and photocatalytic activity, though a comparison of Figure 3b and Figure 11b-c suggests that there is a relationship between reaction yield or *F*/*T* ratio and photocatalytic activity.

The important issue is how particle quality (particle shape and particle size heterogeneity) influences photocatalytic activity. Further studies on the correlation between properties of DAPs and their photocatalytic activity in different reaction systems is going on along this line.

4. Conclusions

The newly developed coaxial-flow gas-phase reactor system used in this study proved to be an efficient system for preparing titania particles with a high content of DAPs. The method ensured high reproducibility and reaction yield of the production of DAP-containing samples with high-level photocatalytic activity, often exceeded photocatalytic activity of one of the most active photocatalyst titania P25. Preparation parameters including concentration of $TiCl_4$ vapor in the reaction zone, furnace temperature and line speed ratio of reaction gases were discussed. The use of a system for continuous $TiCl_4$ feeding enabled precise control of $TiCl_4$ vapor concentration and line speed ratio. Variation in the concentration of $TiCl_4$ allowed stable adjustment of the main physical and structural properties of DAP-containing samples including specific surface area, particle size and particle morphology. It was found

that the concentration of $TiCl_4$ vapor directly influenced particle shape by changing DAP content and particle size heterogeneity. There is a possibility to obtain DAPs with higher SSA by decreasing $C_{TiCl4(g)}$ value. It was shown that the furnace temperature that allows production of titania with a high DAP content (above 50%) and high reaction yield is in the range of 1333 to 1473 K. The line speed ratio of reaction gases is correlated with residence times of gaseous reagents and it influences the gas flow character. This parameter mainly affected reaction yield and particle size heterogeneity. During scaling up procedure of the experimental setup it is important to consider the expected changes in the flow character of gas mixture and its consequences determining the further development of the gas-phase reactor. A high concentration of $TiCl_4$ and a high line speed ratio (low value of residence time) favor production of particles with mounds on {001} facets. The origin of the above-mentioned observation is still ambiguous, but possible explanations are formation of new crystals on the surfaces of existing particles (surface oxidation pathway) or transformation of DAPs to crystals containing high-index facets. Changes in preparation parameters influenced photocatalytic activity. The relationships found between preparation parameters and properties of DAPs show the most favorable ranges of parameters for obtaining high-quality DAPs with a high reaction yield, which may contribute to the scaling up of the preparation process. Correlations of DAP content and particle size heterogeneity with photocatalytic activity were found mainly for the decomposition of acetic acid reaction. More detailed study on the correlations between particle properties and photocatalytic activities is needed to clarify the role of particle shape in the reaction mechanism and for improvement of photocatalytic activity. This research is now in progress.

Acknowledgments

A part of the studies presented in this paper was supported by a Grant-in-Aid (KAKENHI) from the Ministry of Education, Culture, Sports, Science and Technology (MEXT) of Japan (Grant No. 2510750303).

References

[1] M.R. Hoffmann, S.T. Martin, W.Y. Choi, D.W. Bahnemann, Environmental Applications of Semiconductor Photocatalysis, Chem. Rev. 95 (1995) 69-96.

[2] P. Kamat, Meeting the Clean Energy Demand: Nanostructure Architectures for Solar Energy Conversion, J. Phys. Chem. C 111 (2007) 2834-2860.

[3] B. Ohtani, Photocatalysis A to Z—What we know and what we do not know in a scientific sense, J. Photochem. Photobiol. C: Photochem. Rev. 11 (2010) 157-178.

[4] H. Kisch, W. Macyk, Visible-light photocatalysis by modified titania, Chem. Phys. Chem. 3 (2002) 399-400.

[5] E. Kowalska, O.O. Mahaney, R. Abe, B. Ohtani, Visible-light-induced photocatalysis through surface plasmon excitation of gold on titania surfaces, Phys. Chem. Chem. Phys. 12 (2010) 2344-2355.

[6] H. Kisch, S. Sakthivel, M. Janczarek, D. Mitoraj, A low-band gap, nitrogen-modified titania visible-light photocatalyst, J. Phys. Chem. C 111 (2007) 11445-11449.

[7] M.V. Dozzi, E. Selli, Doping TiO_2 with p-block elements: Effects on photocatalytic activity, J. Photochem. Photobiol. C: Photochem. Rev. 14 (2013) 13-28.

[8] B. Ohtani, Preparing articles on photocatalysis—beyond the illusions, misconceptions, and speculation, Chem. Lett. 37 (2008) 217-229.

[9] B. Ohtani, R.M. Bowman, D.P. Colombo, H. Kominami, H. Noguchi, K. Uosaki, Femtosecond diffuse reflectance spectroscopy of aqueous titanium(IV) oxide suspension: correlation of electron-hole recombination kinetics with photocatalytic activity, Chem. Lett. 27 (1998) 579-580.

[10] B. Ohtani, K. Iwai, S. Nishimoto, S. Sato, Role of platinum deposits on titanium(IV) oxide particles: structural and kinetic analyses of photocatalytic reaction in aqueous alcohol and amino acid solutions, J. Phys. Chem. 101 (1997) 3349-3359.

[11] C.J. Chen, C.H. Liao, K.C. Hsu, Y.T. Wu, J.C.S. Wu, P–N junction mechanism on improved NiO/TiO_2 photocatalyst, Catal. Comm. 12 (2011) 1307-1310.

[12] T. Ohno, K. Sarukawa, M. Matsumura, Crystal faces of rutile and anatase TiO_2 particles and their roles in photocatalytic reactions, New J. Chem. 26 (2002) 1167-1170.

[13] A. Selloni, Crystal growth: anatase shows its reactive side, Nat. Mater. 7 (2008) 613-615.

[14] G. Liu, J.C. Yu, G.C. Lu, H.M. Cheng, Crystal facet engineering of semiconductor photocatalysts: motivations, advances and unique properties, Chem. Comm. 47 (2011) 6763-6783.

[15] F. Amano, T. Yasumoto, O.O. Prieto-Mahaney, S. Uchida, T. Shibayama, B. Ohtani, Photocatalytic activity of octahedral single-crystalline mesoparticles of anatase titanium(IV) oxide, Chem. Comm. 45 (2009) 2311-2313.

[16] Z. Wei, E. Kowalska, B. Ohtani, Enhanced photocatalytic activity by particle morphology: preparation, characterization, and photocatalytic activities of octahedral anatase titania particles, Chem. Lett. 43 (2014) 346-348.

[17] F. Amano, O.O. Prieto-Mahaney, Y. Terada, T. Yasumoto, T. Shibayama, B. Ohtani, Decahedral single-crystalline particles of anatase titanium(IV) oxide with high photocatalytic activity, Chem. Mater. 21 (2009) 2601-2603.

[18] F. Amano, T. Yasumoto, O.O. Prieto-Mahaney, S. Uchida, T. Shibayama, Y. Terada, B. Ohtani, Highly active titania photocatalyst particles of controlled crystal phase, size, and polyhedral shapes, Top. Catal. 53 (2010) 455-461.

[19] N. Sugishita, Y. Kuroda, B. Ohtani, Preparation of decahedral anatase titania particles with high-level photocatalytic activity, Catal. Today 164 (2011) 391-394.

[20] X. Han, X. Wang, S. Xie, Q. Kuang, J. Ouyang, Z. Xie, L. Zheng, Carbonate ions-assisted syntheses of anatase TiO_2 nanoparticles exposed with high energy (001) facets, RSC Adv. 2 (2012) 3251-3253.

[21] M.A. Lovette, A.R. Browning, D.W. Griffin, J.P. Sizemore, R.C. Snyder, M.F. Doherty, Crystal shape engineering, Ind. Eng. Chem. Res. 47 (2008) 9812-9833.

[22] H.G. Yang, C.H. Sun, S.Z. Qiao, J. Zou, G. Liu, S.C. Smith, H.M. Cheng, G.Q. Lu, Anatase TiO_2 single crystals with a large percentage of reactive facets, Nature 453 (2008) 638-641.

[23] G. Liu, C. Sun, H.G. Yang, S.C. Smith, L. Wang, G.Q. Lu, H.M. Cheng, Nanosized anatase TiO_2 single crystals for enhanced photocatalytic activity, Chem. Comm. 46 (2010) 755-757.

[24] J. Pan, G. Liu, G.Q. Lu, H.M. Cheng, On the true photoreactivity order of {001}, {010}, and {101} facets of anatase TiO_2 crystals, Angew. Chem. Int. Ed. 50 (2011) 2133-2137.

[25] Y. Alivov, Z.Y. Fan, A method for fabrication of pyramid-shaped TiO_2 nanoparticles with a high {001} facet percentage, J. Phys. Chem. C 113 (2009) 12954-12957.

[26] L. Pan, J.J. Zou, S. Wang, X.Y. Liu, X. Zhang, L. Wang, Morphology evolution of TiO_2 facets and vital influences on photocatalytic activity, ACS Appl. Mater. Interfaces 4 (2012) 1650-1655.

[27] Q. Wu, M. Liu, Z. Wu, Y. Li, L. Piao, Is photooxidation activity of {001} facets truly lower than that of {101} facets for anatase TiO_2 crystals?, J. Phys. Chem. C 116 (2012) 26800-26804.

[28] D. Zhang, G. Li, X. Yang, J.C. Yu, A micrometer-size TiO_2 single-crystal photocatalyst with remarkable 80% level of reactive facets, Chem. Comm. 29 (2009) 4381-4383.

[29] E.J.W. Crossland, N. Noel, V. Sivaram, T. Leijtens, J.A. Alexander-Weber, H.J. Snaith, Mesoporous TiO_2 single crystals delivering enhanced mobility and optoelectronic device performance, Nature 495 (2013) 215-219.

[30] T.R. Gordon, M. Cargnello, T. Paik, F. Magnolini, R.T. Weber, P. Fornasiero, C.B. Murray, Nonaqueous synthesis of TiO_2 nanocrystals using TiF_4 to engineer morphology, oxygen vacancy concentration, and photocatalytic activity, J. Am. Chem. Soc. 134 (2012) 6751-6761.

[31] I.A. Perales-Martinez, V. Rodriguez-Gonzales, S. Obregon-Alfaro, L. Soo-Wohn, Facile synthesis of decahedral particles of anatase TiO_2 with exposed {001} facets, J. Nanosci. Nanotech. 15 (2015) 7351-7356.

[32] H. Li, L. Zhou, L. Wang, Y. Liu, J. Lei, J. Zhang, *In situ* growth of TiO_2 nanocrystals on g-C_3N_4 for enhanced photocatalytic performance, Phys. Chem. Chem. Phys. 17 (2015) 17406-17412.

[33] D.G. Calatayud, T. Jardiel, M. Peiteado, F. Illas, E. Giamello, F.J. Palomares, D. Fernandez-Hevia, A.C. Caballero, Synthesis and characterization of blue faceted anatase nanoparticles through extensive fluorine lattice doping, J. Phys. Chem. C 119 (2015), 21243-21250.

[34] N. Murakami, Y. Kurihara, T. Tsubota, T. Ohno, Shape-controlled anatase titanium(IV) oxide particles prepared by hydrothermal treatment of peroxo titanic acid in the presence of polyvinyl alcohol, J. Phys. Chem. C 113 (2009) 3062-3069.

[35] N. Murakami, S. Kawakami, T. Tsubota, T. Ohno, Dependence of photocatalytic activity on particle size of a shape-controlled anatase titanium(IV) oxide nanocrystal, J. Mol. Catal. A: Chem. 358 (2012) 106-111.

[36] P.P. Ahonen, J. Joutsensaari, O. Richard, U. Tapper, D.P. Brown, J.K. Jokiniemi, E.I. Kauppinen, Mobility size development and the crystallization path during aerosol decomposition synthesis of TiO_2 particles, Aerosol Sci. 32 (2001) 615-630.

[37] P.P. Ahonen, A. Moisala, U. Tapper, D.P. Brown, J.K. Jokiniemi, E.I. Kauppinen, Gas-phase crystallization of titanium dioxide nanoparticles, J. Nanopart. Res. 4 (2002) 43-52.

[38] L. Zhang, Plasma synthesis of metal oxide nanoparticles, US Patent No.7217407 (2007).

[39] G.P. Fotou, T.T. Kodas, B. Anderson, Coating titania aerosol particles with ZrO_2, Al_2O_3/ZrO_2 and SiO_2/ZrO_2 in a gas-phase process, Aerosol Sci. Tech. 33 (2000) 557-571.

[40] B. Ohtani, O.O. Prieto-Mahaney, D. Li, R. Abe, What is Degussa (Evonik) P25? Crystalline composition analysis, reconstruction from isolated pure particles and photocatalytic activity test, J. Photochem. Photobiol. A: Chem. 216 (2010) 179-182.

[41] A. Kayode Coker, Modeling of Chemical Kinetics and Reactor Design, second ed., Gulf Publishing Company, Houston, 2001.

[42] J-G. Li, M. Ikeda, R. Ye, Y Moriyoshi, T. Ishigaki, Control of particle size and phase formation of TiO_2 nanoparticles synthesized in RF induction plasma, J. Phys. D: Appl. Phys. 40 (2007) 2348-2353.

[43] S.E. Pratsinis, P.T. Spicer, Competition between gas phase and surface oxidation of $TiCl_4$ during synthesis of TiO_2 particles, Chem. Eng. Sci. 53 (1998) 1861-1868.

[44] P.T. Spicer, O. Chaoul, S. Tsantilis, S.E. Pratsinis, Titania formation by $TiCl_4$ gas phase oxidation, surface growth and coagulation, Aerosol Sci. 33 (2002) 17-34.

[45] S.C. Garrick, Growth mechanisms of nanostructured titania in turbulent reacting flows, J. Nanotech (2015) Article ID 642014, http://dx.doi.org/10.1155/2015/642014

[46] A.A. Gribb, J.F. Banfield, Particle size effects on transformation kinetics and phase stability in nanocrystalline TiO_2, Am. Mineral., 82 (1997) 717-729.

[47] A.S. Barnard, H. Xu, An environmentally sensitive phase map of titania nanocrystals, ACS Nano 2 (2008) 2237-2242.

[48] Z. Wei, E. Kowalska, B. Ohtani, Influence of post-treatment operations on structural properties and photocatalytic activity of octahedral anatase titania particles prepared by an ultrasonication-hydrothermal reaction, Molecules 19 (2014) 19573-19587.

[49] I.S. Grover, S. Singh, B. Pal, Stable anatase TiO_2 formed by calcination of rice-like titania nanorod at 800°C exhibits high photocatalytic activity, RSC Adv. 4 (2014) 24704-24709.

[50] H.B. Jiang, Q. Cuan, C.Z. Wen, J. Xing, D. Wu, X.Q. Gong, C. Li, H.G. Yang, Anatase TiO_2 crystals with exposed high-index facets, Angew. Chem. Int. Ed. 50 (2011) 3764-3768.

[51] P. Pichat, M.N. Mozzanega, H. Courbon, Investigation of the mechanism of photocatalytic alcohol dehydrogenation over Pt/TiO_2 using poisons and labelled ethanol, J. Chem. Soc. Faraday Trans. 1 83 (1987) 697-704.

[52] C. Liu, X. Han, S. Xie, Q. Kuang, X. Wang, M. Jin, Z. Xie, L. Zheng, Enhancing the photocatalytic activity of anatase TiO_2 by improving the specific facet-induced spontaneous separation of photogenerated electrons and holes, Chem. Asian J. 8 (2013) 282-289.

[53] Z. Wei, E. Kowalska, J. Verret, C. Colbeau-Justin, H. Remita, B. Ohtani, Morphology-dependent photocatalytic activity of octahedral anatase particles prepared by ultrasonication-hydrothermal reaction of titanates, Nanoscale 7 (2015) 12392-12404.

Table 1
Controlled (U, p, T_F), resultant (C_{TiCl4}, LSR) and gas flow (Re, t_{res}) parameters for gas-phase preparation of DAPs.

$C_{TiCl4(g)}$ (vol%)	LSR	T_F /K	U_{TiCl4} /mL h^{-1}	U_{O2} /mL min^{-1}	U_{Ar} /mL min^{-1}	p /kPa	Re	t_{res} /s
0.34	0.08	1373	0.6	1000	75	95	9.5	0.98
0.86	0.08	1373	1.5	1000	75	95	10.2	0.98
1.30	0.08	1373	2.5	1100	75	95	11.5	0.89
2.13	0.08	1373	5.0	1350	75	95	15.0	0.73
0.86	0.04	1373	3.2	2200	75	95	21.5	0.46
0.86	0.06	1373	2.2	1500	75	95	14.8	0.67
0.86	0.08	1373	1.5	1000	75	95	10.2	0.98
0.86	0.12	1373	1.0	650	75	95	6.7	1.45
0.86	0.16	1373	0.8	500	75	95	5.3	1.83
0.86	0.08	1173	1.5	1000	75	95	11.0	1.14
0.86	0.08	1273	1.5	1000	75	95	10.5	1.05
0.86	0.08	1333	1.5	1000	75	95	10.2	1.00
0.86	0.08	1373	1.5	1000	75	95	10.0	0.98
0.86	0.08	1473	1.5	1000	75	95	9.6	0.91

List of figures

Fig. 1. Experimental system for gas-phase preparation of DAP-containing samples: (1) vaporizer with heating hood, (2) automatic syringe feeder, (3) preheating-zone tube, (4) quartz reaction tube, (5) infrared furnace, (6) platinum foil, (7) vacuum pump, (8) pressure regulator with a vacuum gauge, (9) dessicator tube with silica gel packing, (10) shower-type scrubber, (11) peristaltic pump, (12) glass-fiber filter, (13) reservoir of an aqueous sodium hydroxide solution, (T-1) vaporizer heating zone, (T-2) preheating zone of gases, (T-3) reaction heating zone.

Fig. 2. SEM images of particles classified into different categories of particle shape distribution analysis: (A) DAP, (B) semi-DAP (mounds), (C) semi-DAP (aggregates), (D) semi-DAP (other), (E) others.

Fig. 3. Influence of (a) $C_{TiCl4(g)}$, (b) *LSR* and (c) T_F on reaction yield (■) and *F*/*T* ratio (□). Relationship between reaction yield and *F*/*T* ratio (d).

Fig. 4. Relationships of residence time with reaction yield (■) and *F*/*T* ratio (□). The shaded area indicates the range of residence times of 0.8–1.0 s.

Fig. 5. Relationships of $C_{TiCl4(g)}$ with *SSA* (■), *PPS* (□) and *SPS* (○).

Fig. 6. Relationships of (a) $C_{TiCl4(g)}$, (b) *LSR* and (c) T_F with *PSH*.

Fig. 7. Influence of the *Re* value on *PSH*.

Fig. 8. XRD diffractograms of a typical DAP-containing sample (a) pure (b) mixed with NiO.

Fig. 9. Influence of (a) $C_{TiCl4(g)}$, (b) *LSR* and (c) T_F on *PSD*: DAP (■), semi-DAP (●) and others (▲).

Fig. 10. SEM images of DAP-containing samples prepared with different $TiCl_4$ vapor concentrations: (A) 0.34vol%, (B) 0.86vol%, (C) 1.30vol% and (D) 2.13vol%. "A": particle aggregates, "M": a mound located on the {001} facet.

Fig. 11. Influence of (a) $C_{TiCl4(g)}$, (b) *LSR* and (c) T_F on photocatalytic activities in the CO_2 system (■) and H_2 system (□). Photocatalytic activities were standardized with reference to the photocatalytic activity of P25.

Fig. 12. Influence of (a) DAP content, (b) content of particles with mounds in the CO_2 system (■) and H_2 system (□). Photocatalytic activities were standardized with reference to the photocatalytic activity of P25.

Figure 1

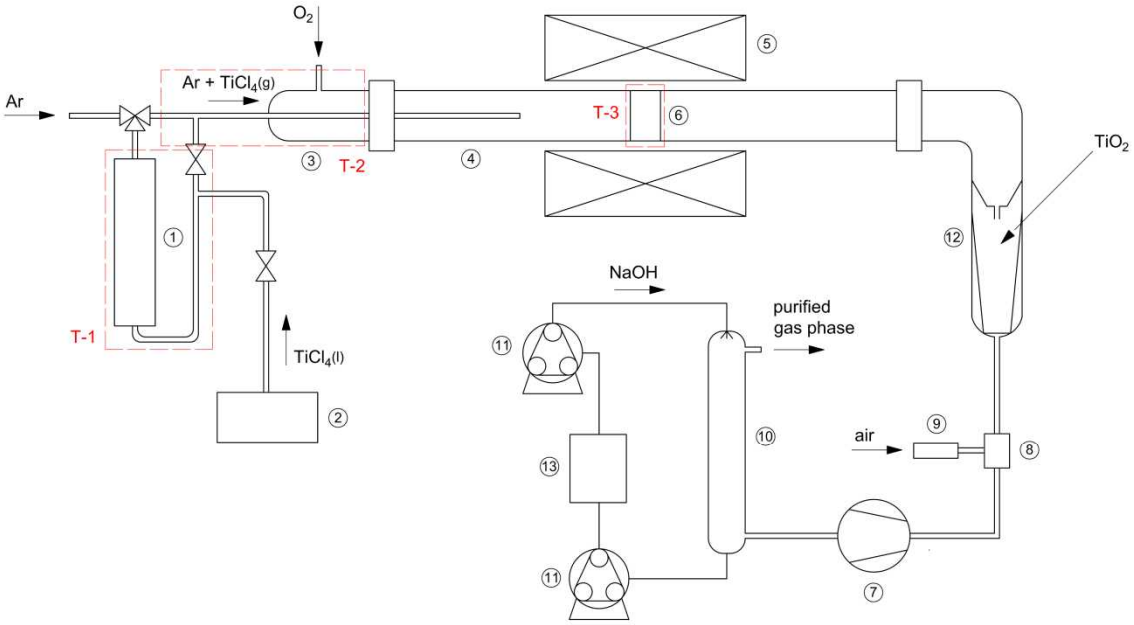
O2
Ar
Ar + TiCl4(g)
T-1
T-2
T-3
TiCl4(l)
NaOH
purified
gas phase
air
TiO2
1
2
3
4
5
6
7
8
9
10
11
12
13

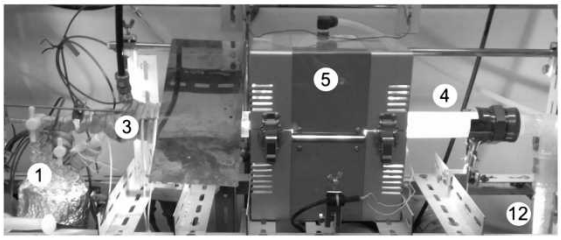
1
3
4
5
12

Figure 2

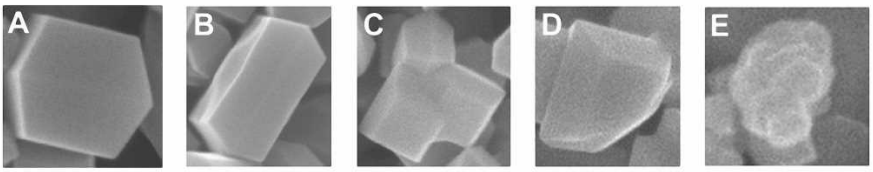

Figure 3

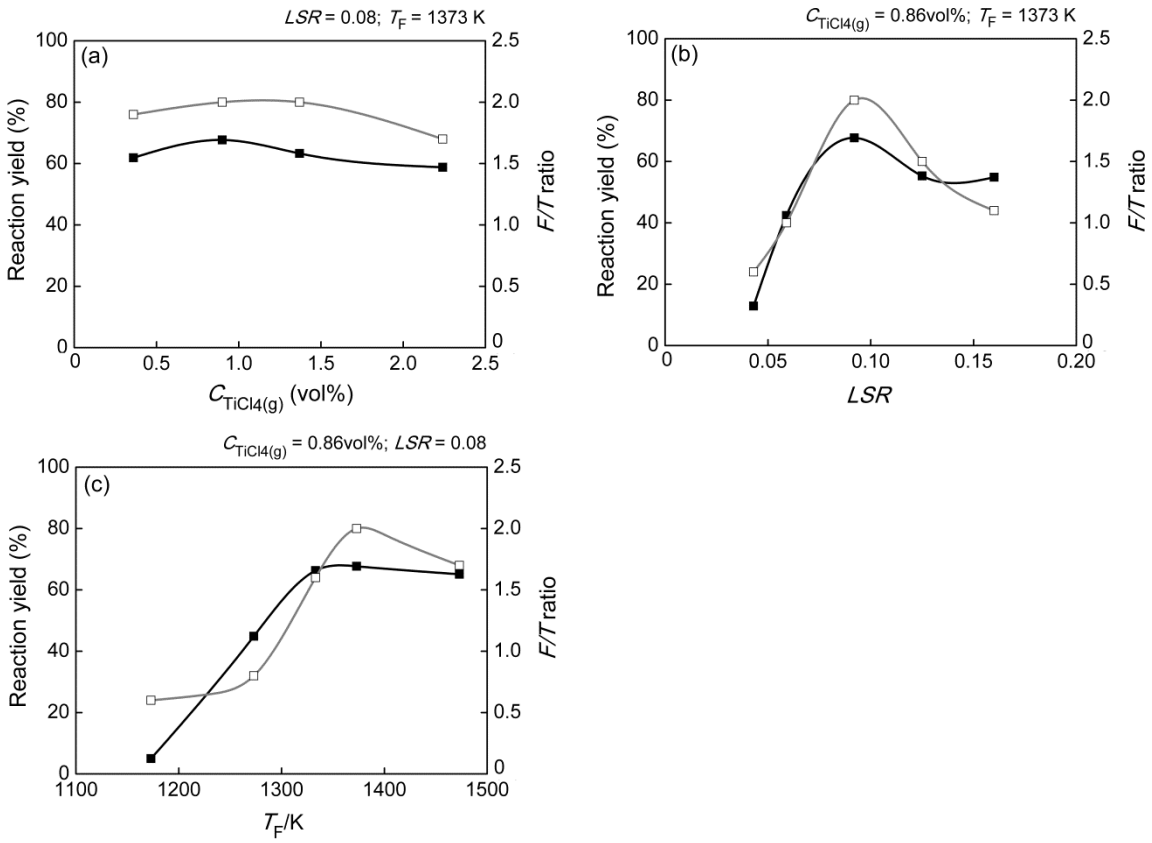
LSR = 0.08; T_F = 1373 K
(a)
Reaction yield (%)
F/T ratio
C_TiCl4(g) (vol%)
C_TiCl4(g) = 0.86vol%; T_F = 1373 K
(b)
LSR
C_TiCl4(g) = 0.86vol%; LSR = 0.08
(c)
T_F/K

Figure 4

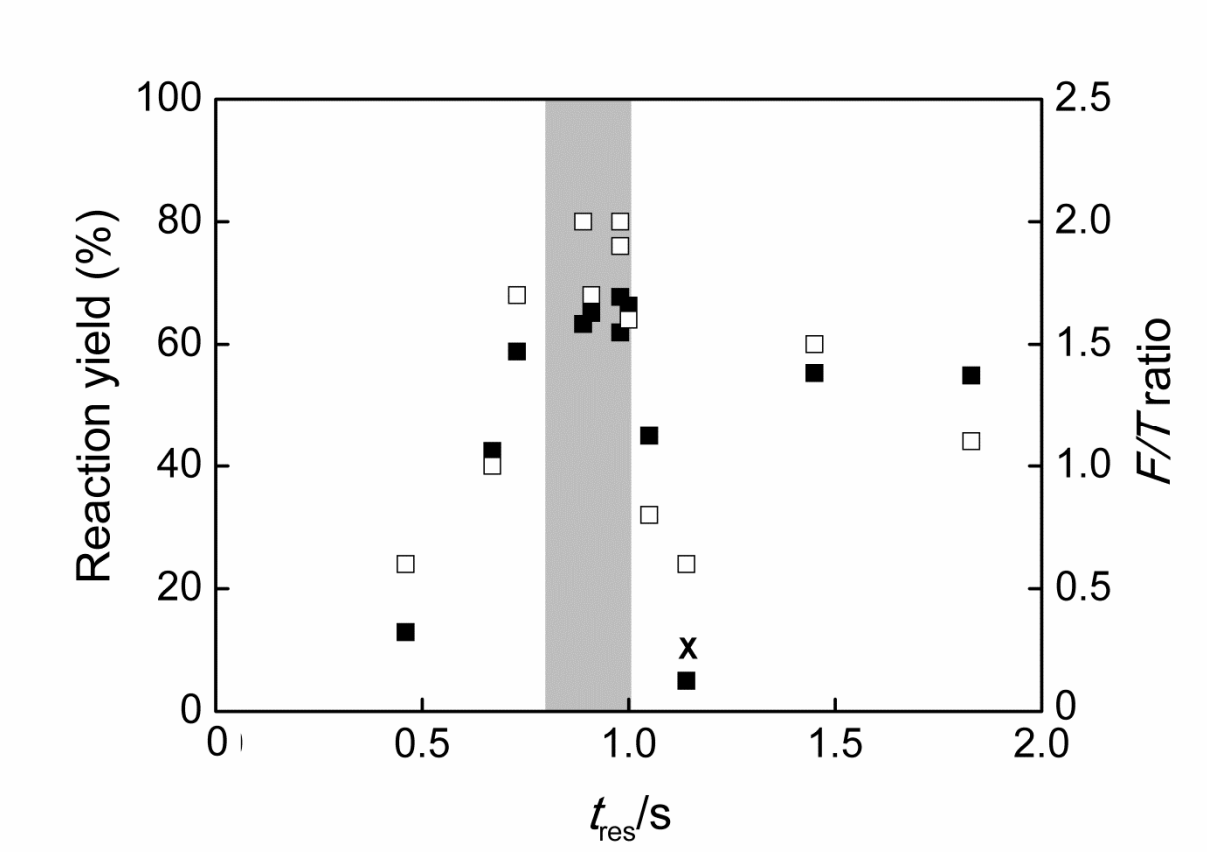

Figure 5

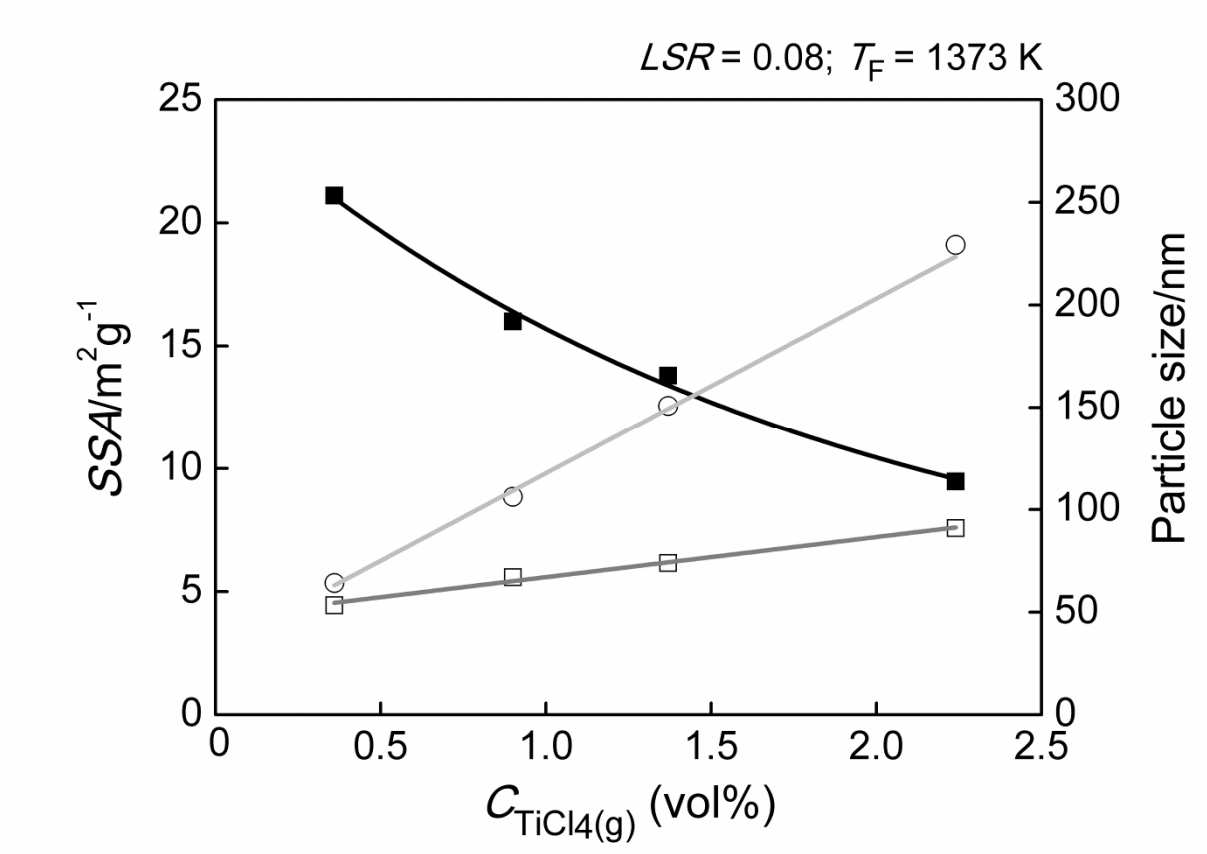
LSR = 0.08; T_F = 1373 K
SSA/m²g⁻¹
Particle size/nm
C_TiCl4(g) (vol%)
0
5
10
15
20
25
0
50
100
150
200
250
300
0
0.5
1.0
1.5
2.0
2.5

Figure 6

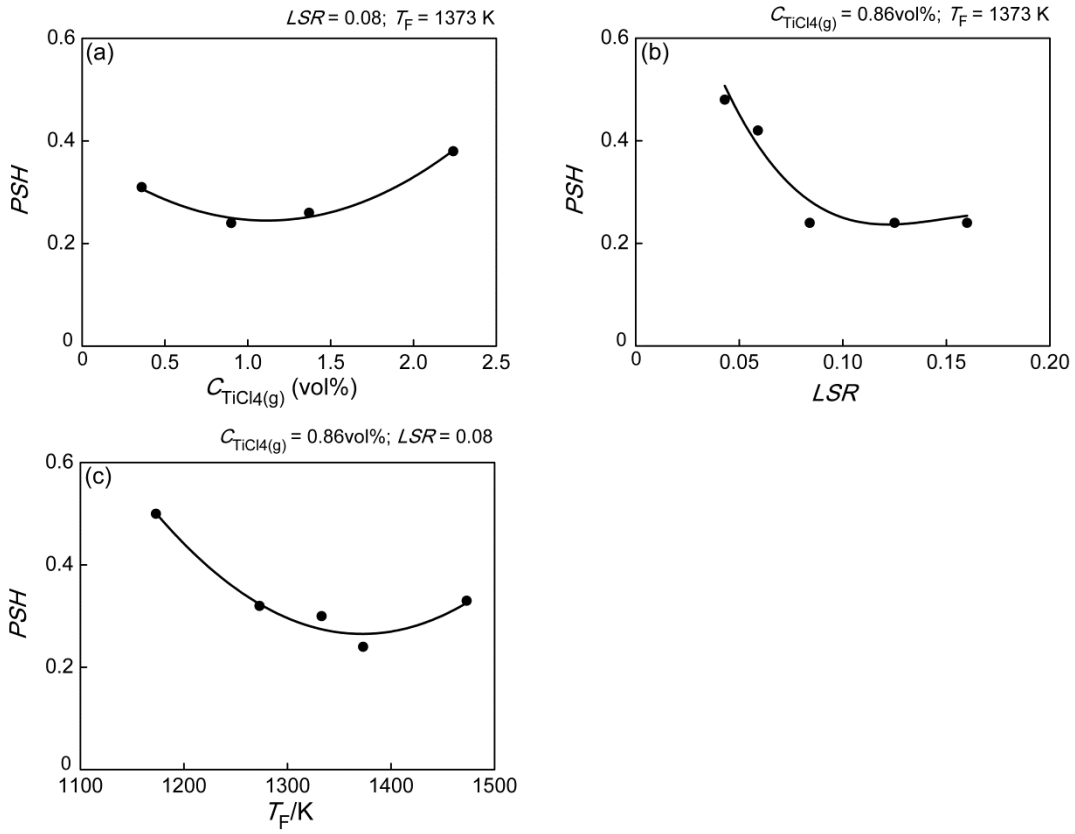
LSR = 0.08; T_F = 1373 K
(a)
PSH
C_TiCl4(g) (vol%)
C_TiCl4(g) = 0.86vol%; T_F = 1373 K
(b)
PSH
LSR
C_TiCl4(g) = 0.86vol%; LSR = 0.08
(c)
PSH
T_F/K

Figure 7

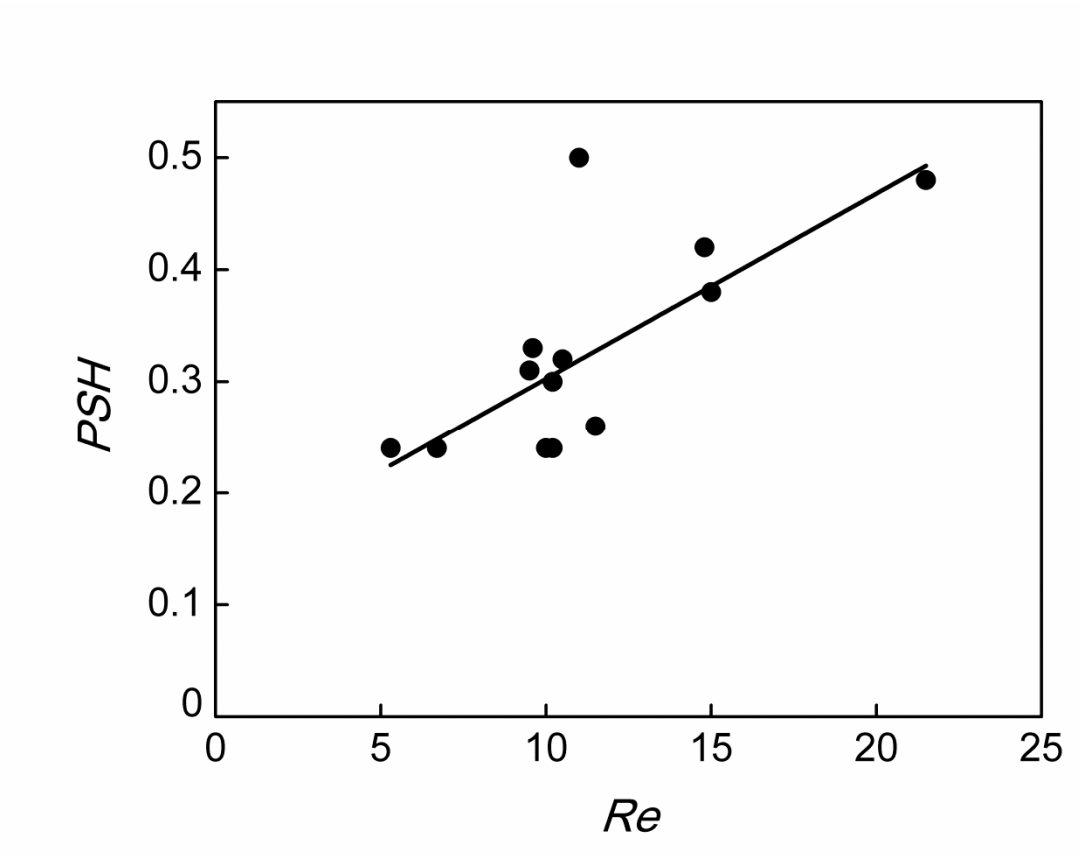

Figure 8

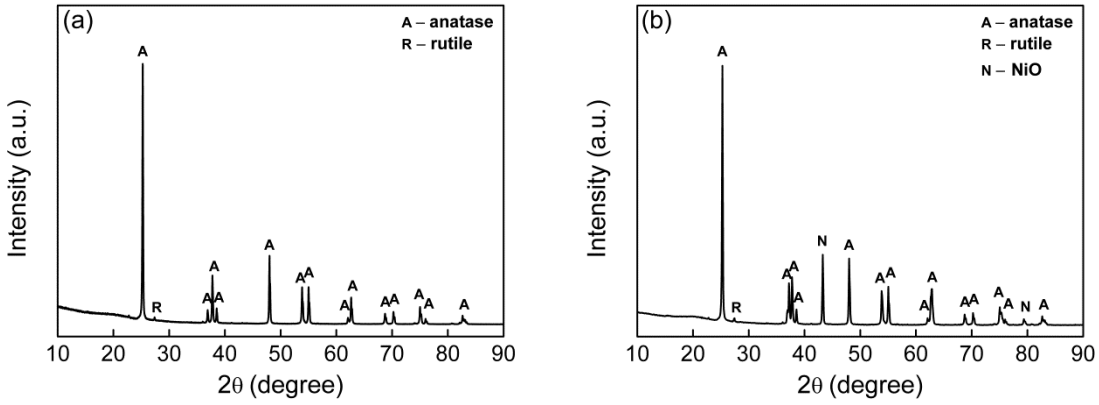
(a)
A – anatase
R – rutile
Intensity (a.u.)
2θ (degree)
(b)
A – anatase
R – rutile
N – NiO
Intensity (a.u.)
2θ (degree)

Figure 9

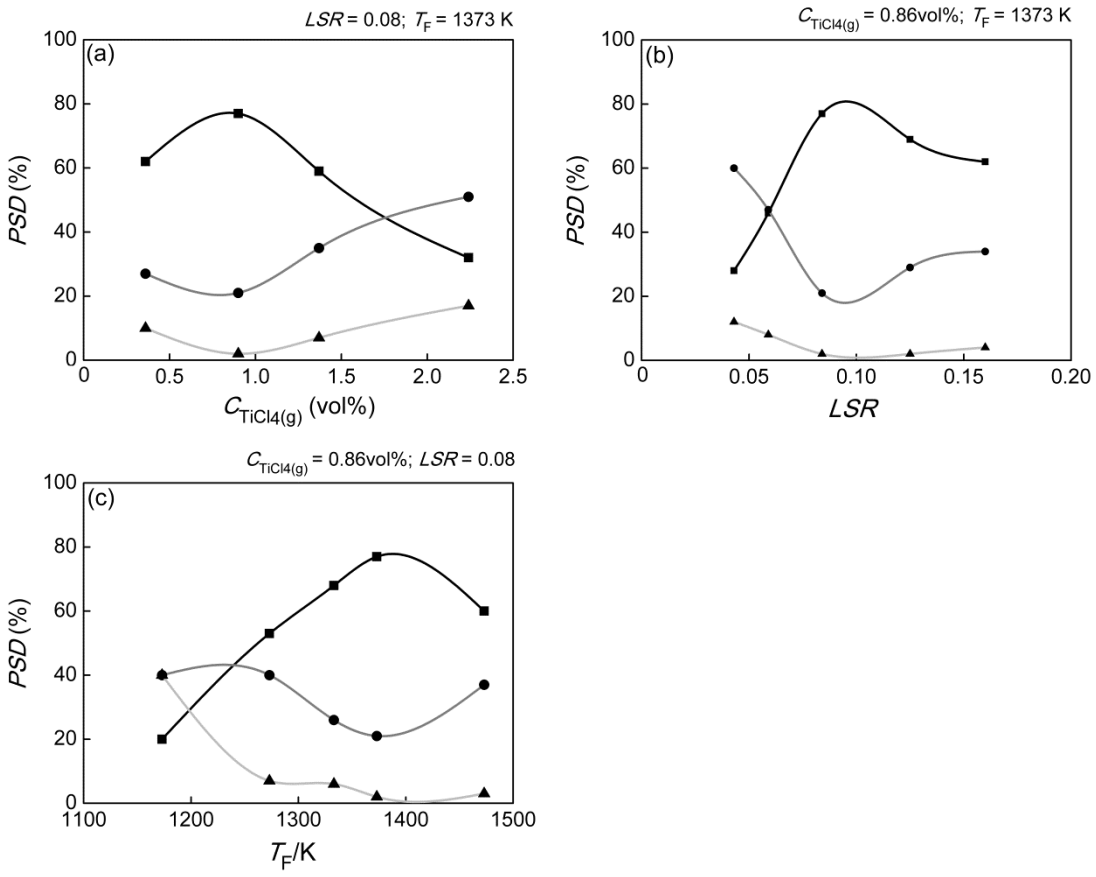
LSR = 0.08; T_F = 1373 K
(a)
PSD (%)
C_TiCl4(g) (vol%)
C_TiCl4(g) = 0.86vol%; T_F = 1373 K
(b)
PSD (%)
LSR
C_TiCl4(g) = 0.86vol%; LSR = 0.08
(c)
PSD (%)
T_F/K

Figure 10

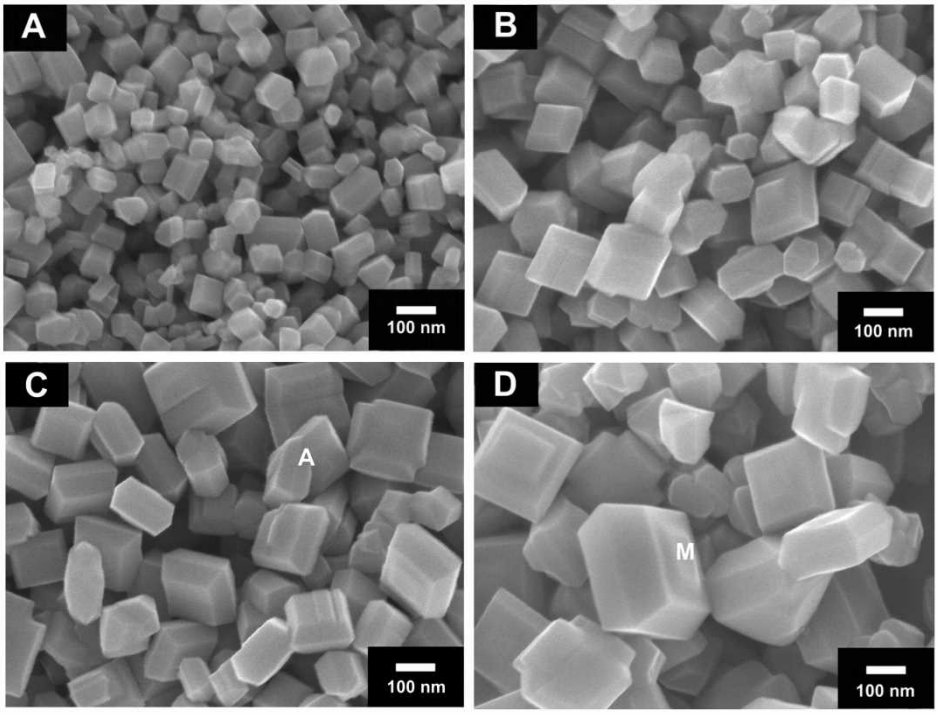

Figure 11

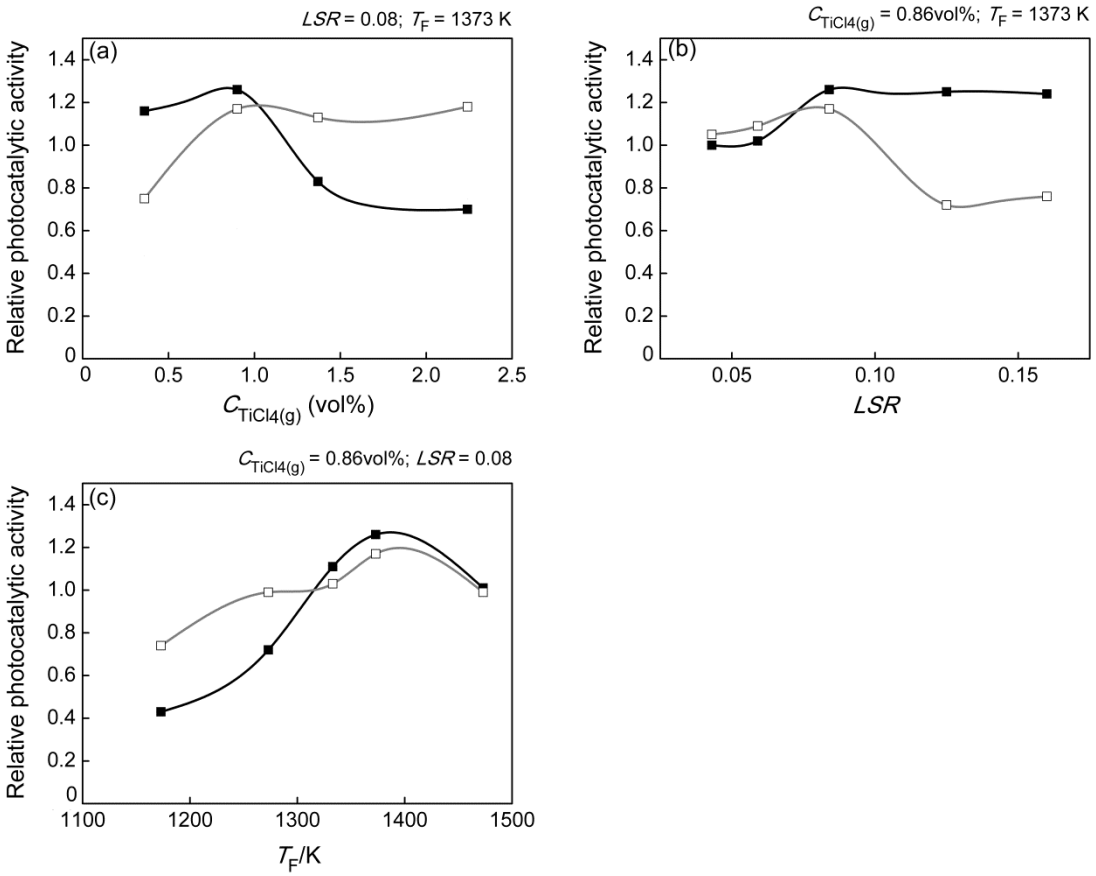
LSR = 0.08; T_F = 1373 K
(a)
Relative photocatalytic activity
C_TiCl4(g) (vol%)
C_TiCl4(g) = 0.86vol%; T_F = 1373 K
(b)
Relative photocatalytic activity
LSR
C_TiCl4(g) = 0.86vol%; LSR = 0.08
(c)
Relative photocatalytic activity
T_F/K

Figure 12

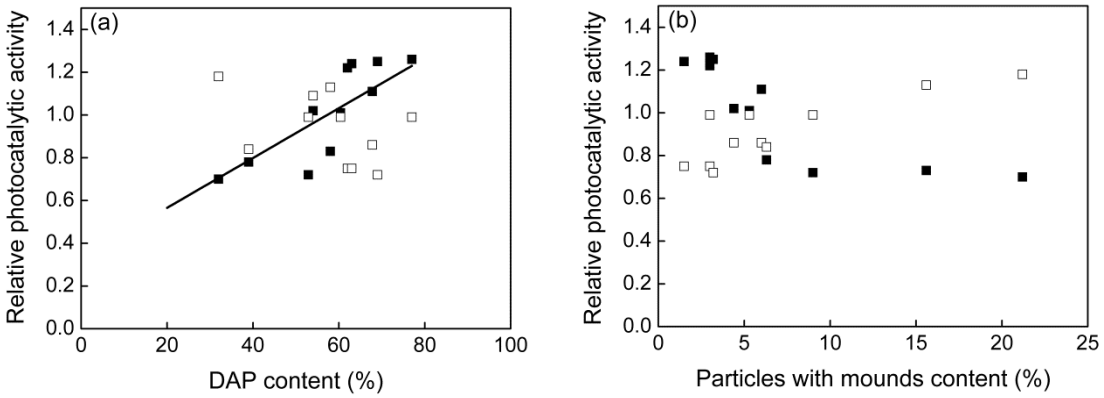
(a)
Relative photocatalytic activity
DAP content (%)
(b)
Relative photocatalytic activity
Particles with mounds content (%)